Lamellae Alignment by Shear Flow in a Model of a Diblock Copolymer

François Drolet[†] and Peilong Chen[‡]

Supercomputer Computations Research Institute, Florida State University, Tallahassee, Florida 32306-4130

Jorge Viñals*

Supercomputer Computations Research Institute, Florida State University, Tallahassee, Florida 32306-4130, and Department of Chemical Engineering, Florida A&M University−Florida State University College of Engineering, Tallahassee, Florida 32310-6046

Received March 25, 1999; Revised Manuscript Received September 16, 1999

ABSTRACT: A mesoscopic model of a diblock copolymer is used to study the stability of a lamellar structure under a uniform shear flow. We first obtain the nonlinear lamellar solutions under both steady and oscillatory shear flows. Regions of existence of these solutions are determined as a function of the parameters of the model and of the flow. Finally, we address the stability of the lamellar solution against long-wavelength perturbations.

1. Introduction

We study a mesoscopic model of a block copolymer to describe the reorientation of a lamellar structure by an imposed uniform shear flow that is either constant or periodic in time. This is the first step toward understanding known phenomenology pertaining to the response of the block copolymer microstructure to shear flows near the isotropic to lamellar transition.[1] The model that we use is based on the free energy of the diblock copolymer obtained by Leibler,[2] and later by Ohta and Kawasaki,[3] to which an advection term is added to incorporate the effect of the externally applied shear flow. We identify spatially periodic solutions that correspond to a lamellar structure, and determine their stability against a number of long-wavelength perturbations.

Modulated phases are ubiquitous in physical and chemical systems.[4] They generally result from the competition between short- and long-range forces. Additional symmetries of the system (e.g., translational or rotational invariance) often lead in practice to rich textures, especially in systems of extent that is large compared with the characteristic wavelength of the modulation. Modulated phases often have interesting macroscopic behavior, and exhibit a complex response to externally applied forces. While it is possible to devise approximate constitutive laws to describe the macroscopic response of such phases, it is often necessary to explicitly address their evolution at the mesoscopic scale, and to determine how microstructure evolution influences the macroscopic response.

We focus here on the lamellar phase observed in diblock copolymers below the order−disorder transition.[2,3,5] Diblock copolymers are formed by two distinct sequences of monomers, A and B, that are mutually incompatible but chemically linked. At sufficiently low temperatures, species A and B would segregate to form macroscopic domains, but the chemical bonding between the two leads to a modulated phase instead. The detailed equilibrium microstructure depends on the relative molecular weight of the chains[2,3,6,7] and has been studied in detail within a mean field approximation.[8,9]

We follow in this paper the approach of Leibler who introduced an order parameter field $\psi(\mathbf{r})$ that describes the local number density difference of monomers A and B. The order parameter is defined to be zero above the order−disorder transition, and is finite and nonuniform below. Leibler's analysis was restricted to the weak-segregation limit (close to the order−disorder transition) within which the thickness of the interface separating the A-rich from the A-poor regions is on the order of the wavelength of the microstructure. Later, Ohta and Kawasaki extended Leibler's free energy to the strong-segregation range, and showed the importance of long-ranged effective interactions that arise from the connectivity of the polymer chains. We use this latter free energy as the driving force for the reorientation dynamics, allowing also for passive advection of the order parameter by an imposed shear flow. The model studied is similar to that considered by Fredrickson,[10] except that we neglect thermal fluctuations and assume that both phases have the same viscosity.

The stability of a lamellar structure to secondary instabilities has already been addressed in the literature, although in the absence of shear flow.[11,12] In fact, the similarity between the equations governing the motion of the lamellae and the Swift−Hohenberg model of Rayleigh−Bénard convection[13−15] gives rise to a common phenomenology.[12] The lamellar structure is found to be stable only within a range of wavenumbers. At higher wavenumbers it undergoes an Eckhaus instability which generally results in a decrease of wavenumber, whereas for wavenumbers below that range the structure undergoes a zigzag instability. In this paper, we extend these stability results to explicitly include fluid advection by the imposed shear. We find that the stability boundaries are modified with respect to the zero velocity case in a way that depends not only on the amplitude and frequency of the shear, but also on the orientation of the lamellae relative to the flow.

[†] Present and permanent address: Materials Research Laboratory, University of California, Santa Barbara, CA 93106.

[‡] Permanent address: Department of Physics, National Central University, Chungli 320, Taiwan.

10.1021/ma990448o CCC: $18.00
Published on Web 11/13/1999

Of course, the latter dependence is absent in earlier treatments that neglected advection.

Our results are the first step toward understanding the complex reorientation phenomenology that has been observed experimentally.[1] In this initial analysis, we introduce a number of restrictive assumptions that we plan to relax in future work. First, our calculations are primarily two dimensional and thus can only address the so-called parallel and transverse orientations. Second, and more importantly, we neglect thermal fluctuations and any viscosity contrast between the two phases, elements that have been argued to be important in determining the main qualitative features of the reorientation process. We also neglect flow induced by the lamellae themselves in response to the applied shear. These secondary flows could become important for the late-stage coarsening of the lamellar structure. Furthermore, we have confined our study to locating the boundaries of several secondary instabilities of the lamellar structure, but have not addressed the evolution following the instabilities, nor the coarsening of the resulting textured pattern.[16,17] Finally, it has been argued that the motion of defects and grain boundaries under shear plays a crucial role in the alignment process.[18] This mechanism is completely ignored in our study, which focuses on the evolution of a single, perfectly aligned lamellar domain. Nevertheless, our results concerning the periodic base solution under flow, and its stability against long-wavelength perturbations, are the prerequisite building blocks of a more general theory.

2. Mesoscopic Model Equations

Following Leibler,[2] we introduce an order parameter field, $\psi(\mathbf{r})$, function of the local density difference of monomers A and B. For a block copolymer with equal length subchains, the order parameter is $\psi(\mathbf{r}) = [\rho_A(\mathbf{r}) - \rho_B(\mathbf{r})]/2\rho_0$, where ρ_X, X = *A*, *B*, is the density of monomer X, and ρ_0 is the total density, assumed constant (incompressibility condition). A mean field free energy $F[\psi(\mathbf{r})]$ was derived by Leibler for a monodisperse diblock copolymer melt,[2] and later by Ohta and Kawasaki.[3] In units of k_BT, where k_B is Boltzmann's constant and T the temperature, the free energy is comprised of two terms, $F/(\rho_0 k_B T) = F_s + F_l$. The term F_s incorporates local monomer interactions

$$F_s = \int d\mathbf{r} \left[\frac{\kappa}{2}\left|\nabla\psi\right|^2 - \frac{\tau}{2}\psi^2 + \frac{u}{4}\psi^4\right]$$

and is formally identical to the Ginzburg−Landau free energy commonly used to describe phase separation in a binary fluid mixture.[19] Long-range interactions arising from the covalent bond connecting the two subchains are contained in F_l

$$F_l = (B/2)\int\int d\mathbf{r}\, d\mathbf{r}'\, G(\mathbf{r}-\mathbf{r}')\,\psi(\mathbf{r})\,\psi(\mathbf{r}')$$

where the kernel $G(\mathbf{r}-\mathbf{r}')$ is the infinite space Green's function of the Laplacian operator $\nabla^2 G(\mathbf{r}-\mathbf{r}') = -\delta(\mathbf{r}-\mathbf{r}')$. The parameters κ, τ, and B can be approximately related to the polymerization index N, Kuhn's statistical length b, and the Flory−Huggins parameter χ through the relations $\kappa = b^2/3$, $\tau = (2\chi N - 7.2)/N$, and $B = 144/N^2b^2$.[11] The nonlocal interactions arising from the connectivity of the chains lead to a thermodynamic equilibrium state with a nonuniform density. In our case of equal length subchains, the equilibrium configuration is a periodic lamellar structure, with a characteristic wavelength on the order of 100 Å for a typical system.

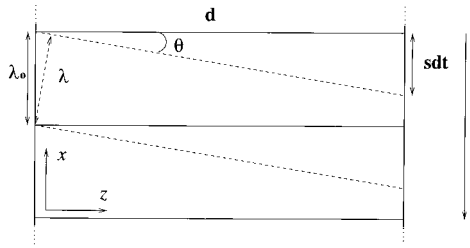

Figure 1. Schematic representation of the configuration studied. We also show a schematic of the distortion of a lamellar pattern under uniform shear flow. The imposed velocity field is along the x direction. The velocity is specified at the $z = d$ boundary, and vanishes at $z = 0$. The lamellae in this graph are transverse to the flow at $t = 0$ (solid lines). At a later time (dotted lines) the lamellae are at an angle with respect to the flow, and the wavelength has changed accordingly.

Given this mean field free energy, a phenomenological set of equations that govern the temporal relaxation of equilibrium thermal fluctuations of $\psi(\mathbf{r})$ and of fluid velocity $\mathbf{v}$ has been derived close to the order−disorder transition.[10,20,21] A similar phenomenological description can be used below the order−disorder transition under the assumption that the local relaxation of the order parameter field at the mesoscopic scale is still driven by minimization of the same free energy.[22−24] Under this assumption, ψ obeys the time-dependent Ginzburg−Landau equation

$$\frac{\partial\psi}{\partial t} + \mathbf{v}\cdot\nabla\psi = M\nabla^2\frac{\delta F}{\delta\psi} \qquad (1)$$

where M is a phenomenological mobility coefficient, $\delta/\delta\psi$ stands for functional differentiation with respect to ψ, and $\mathbf{v}$ is a local velocity field. We focus on a layer of block copolymer, unbounded in the x and y directions, and being uniformly sheared along the z direction (Figure 1). The layer is confined between the stationary $z = 0$ plane and the plane $z = d$, which is uniformly displaced parallel to itself with a velocity $v_{plane} = sd$ in the case of a steady shear, and $v_{plane} = \gamma d\omega\cos(\omega t)$ in the case of an oscillatory shear. s is the dimensional shear rate in the steady case, and γ is the dimensionless strain amplitude in the case of an oscillatory shear of angular frequency ω. Under typical experimental conditions, inertia is negligible ($\omega d^2/\nu \ll 1$, where ν is the kinematic viscosity of the fluid). If we further neglect flow induced by the lamellae themselves, the velocity field is given by $\mathbf{v} = sz\hat{\imath}$ for a steady shear, and $\mathbf{v} = \gamma d\omega\cos(\omega t)\, z\hat{\imath}$ for an oscillatory shear, where $\hat{\imath}$ is the unit vector in the x direction. As discussed in the Introduction, previous theoretical work on the formation and stability of lamellar structures further neglected advection of ψ in eq 1. The results presented in this paper are free of this restriction.

Since the base state to be considered is comprised of spatially uniform lamellae advected by the shear flow, it is convenient to introduce a new frame of reference in which the velocity vanishes. Define a new system of nonmutually orthogonal coordinates (x_1, x_2, x_3) by $x_1 = x - a(t)z$, $x_2 = y$, and $x_3 = z$. The dimensionless quantity $a(t) = st$ for a steady shear, and $a(t) = \gamma\sin(\omega t)$ for an oscillatory shear. All the calculations reported in this paper, both analytical and numerical, have been per-

formed in this new frame of reference. Analytical calculations consider an unbounded geometry in the x_1 and x_2 directions and periodic boundary conditions along the x_3 direction, whereas the numerical computations have been conducted in a two-dimensional, square domain on the (x_1, x_3) plane and consider periodic boundary conditions along both x_1 and x_3. Note that both frames of reference coincide at $t = 0$, and at equal successive intervals of half the period of the shear in the case of oscillatory shear.

Dimensionless variables are introduced by defining a scale of length by $(\kappa/\tau)^{1/2}$, a scale of time by $\kappa/M\tau^2$, and an order parameter scale by $(\tau/u)^{1/2}$. In the transformed frame of reference and in dimensionless variables, eq 1 reads

$$\frac{\partial\psi}{\partial t} = \nabla'^2(-\psi + \psi^3 - \nabla'^2\psi) - \frac{B\kappa}{\tau^2}\psi \qquad (2)$$

with

$$\nabla'^2 = [1 + a^2(t)]\frac{\partial^2}{\partial x_1^2} - 2a(t)\frac{\partial^2}{\partial x_1 \partial x_3} + \frac{\partial^2}{\partial x_3^2} + \frac{\partial^2}{\partial x_2^2}$$

There is only one dimensionless group remaining, $B\kappa/\tau^2$, which will be simply denoted by B in what follows.

We will first show in section 3 that below (but close to) the order−disorder transition point (in the weak-segregation limit), eq 2 admits periodic solutions. Their stability against infinitesimal long-wavelength perturbations is the subject of section 4.

3. Lamellar Solution in the Weak-Segregation Limit

In the absence of shear ($a(t) = 0$) the uniform solution of eq 2, $\psi = 0$, loses stability at the order−disorder transition. In a mean field approximation the transition occurs at $B_c = 1/4$. This is a supercritical bifurcation with a critical wavenumber $q_c = (1/2)^{1/2}$. Near threshold ($0 \le \epsilon = (B_c - B)/2B_c \ll 1$) there exist periodic stationary solutions of the form

$$\psi(\mathbf{r}) = 2A\cos(\mathbf{q}\cdot\mathbf{r}) + A_1\cos(3\mathbf{q}\cdot\mathbf{r}) + ... \qquad (3)$$

with $A^2 = (q^2 - q^4 - B)/3q^2 \approx O(\epsilon)$ and A_1 of higher order in ϵ. This solution only exists for a range of wavenumbers q such that $\sigma(q^2) = q^2 - q^4 - B \ge 0$.

For nonzero shear, we seek solutions of eq 2 of the form of eq 3, with $\mathbf{r} = (x_1, x_2, x_3)$ expressed in the sheared frame basis set $\{\mathbf{e}_1 = \hat{\imath},\ \mathbf{e}_2 = \hat{\jmath},\ \mathbf{e}_3 = a(t)\hat{\imath} + \hat{k}\}$. Wavevectors are expressed in the reciprocal basis set $\{\mathbf{g}_1 = \hat{\imath} - a(t)\hat{k},\ \mathbf{g}_2 = \hat{\jmath},\ \mathbf{g}_3 = \hat{k}\}$. Therefore, we keep the same functional form as for nonzero shear, but allow a time-dependent amplitude $A(t)$. Note that the components of the wavevector $\mathbf{q}$ are assumed to be independent of time and given by $q_1 = q_x(t{=}0)$, $q_2 = q_y(t{=}0)$, and $q_3 = q_z(t{=}0)$, respectively. The wavevector itself depends on time through the time dependence of the reciprocal basis set. Such a solution corresponds to a spatially uniform lamellar structure with a time-dependent wavevector that adiabatically follows the imposed shear in the laboratory frame (see Figure 1). Inserting eq 3 into eq 2, we find to order $\epsilon^{3/2}$ (σ is itself of order ϵ)

$$\mathrm{d}A/\mathrm{d}t = \sigma[q^2(t)]A - 3q^2(t)A^3 \qquad (4)$$

with $q^2(t) = {q_1}^2 + (a(t)q_1 - q_3)^2 + {q_2}^2$ and $\sigma(q^2) = q^2 - q^4 - B$. This nonlinear equation with time-dependent coefficients can be solved exactly in the two cases of steady and oscillatory shear flow.

In the case of a steady shear, $a(t) = st$. We find

$$A(t) = \left\{\frac{\mathrm{e}^{2H(t)}}{A(0)^2} + 6\mathrm{e}^{2H(t)}\int_0^t \mathrm{d}t'\ \mathrm{e}^{-2H(t')}\ q^2(t')\right\}^{-1/2} \qquad (5)$$

with

$$H(t) = ({q_0}^4 + B - {q_0}^2)t + (1 - 2{q_0}^2)\,sq_1q_3t^2 + \frac{2{q_1}^2s^2(2{q_3}^2 + {q_0}^2)}{3}t^3 - {q_1}^3q_3s^3t^4 + \frac{{q_1}^4s^4}{5}t^5 \qquad (6)$$

The constant quantity $q_0 = ({q_1}^2 + {q_2}^2 + {q_3}^2)^{1/2}$ is the initial wavenumber, and $A(0)$ is the initial amplitude. For the special case $q_1 = 0$, $A(t)$ simply relaxes to its equilibrium value in the absence of shear, $A^2 = ({q_0}^2 - {q_0}^4 - B)/3{q_0}^2$. This corresponds to an initial orientation of the structure which has no component transverse to the flow. For any other initial orientation, the shear induces changes in the lamellar spacing in the laboratory frame of reference (Figure 1). As a result, the amplitude $A(t)$ decreases and approaches zero at long times. Hence, the structure melts and re-forms with a different orientation which we cannot predict on the basis of our single-mode analysis. The emerging structure presumably results from the amplification of thermal fluctuations near the point at which the amplitude $A(t)$ vanishes, and they have been neglected in our treatment. Thermal fluctuation effects have been accounted for by others.[10,25]

For an oscillatory shear, $\alpha(t) = \gamma\ \sin(\omega t)$. We first examine the stability of the uniform solution $\psi = 0$ against small perturbations. Linearization of eq 4 leads to

$$\mathrm{d}A(t)/\mathrm{d}t = \sigma[q^2(t)]\ A(t) \qquad (7)$$

with $\sigma(t+T) = \sigma(t)$ and $T = 2\pi/\omega$. Equation 7 constitutes a one-dimensional Floquet problem. The solution $A = 0$ is unstable when

$$\bar{\sigma} = \int_0^T \sigma(t)\ \mathrm{d}t > 0 \qquad (8)$$

The resulting neutral stability curve is given by

$$B = {q_0}^2 - {q_0}^4 - \frac{3{q_1}^4\gamma^4}{8} - \frac{(2{q_0}^2 + 4{q_3}^2 - 1)\gamma^2{q_1}^2}{2} \qquad (9)$$

Instability modes can be conveniently classified by considering the relative orientation of the lamellae at $t = 0$ and the shear direction. We define a parallel orientation, $q_3 \neq 0$, $q_1 = q_2 = 0$, a perpendicular orientation, $q_2 \neq 0$, $q_1 = q_3 = 0$, and a transverse orientation, $q_1 \neq 0$, $q_2 = q_3 = 0$. The following instability points are identified depending on the orientation of the critical wavevector: a transverse mode with

$$B_c = \frac{1}{2}\frac{(2 + \gamma^2)^2}{8 + 8\gamma^2 + 3\gamma^4}, \qquad q_{1c} = \left(\frac{4 + 2\gamma^2}{8 + 8\gamma^2 + 3\gamma^4}\right)^{1/2} \qquad (10)$$

a mixed parallel−perpendicular mode with

$$B_c = 1/4, \qquad q_{1c} = 0, \qquad 2{q_{2c}}^2 + 2{q_{3c}}^2 = 1 \qquad (11)$$

and a mixed parallel−transverse mode defined by

$$B_c = \frac{1}{4}\frac{7\gamma^2+16}{15\gamma^2+16}, \quad q_{2c} = 0, \quad q_{1c} = 2\left(\frac{1}{15\gamma^2+16}\right)^{1/2}, \quad q_{3c} = \left(\frac{3\gamma^2+8}{30\gamma^2+32}\right)^{1/2} \tag{12}$$

Note that the threshold corresponding to perturbations of wavevectors that do not have a projection along the transverse direction are not affected by the shear. Furthermore, neither the stability boundaries nor the values of the critical wavenumbers depend on the angular frequency ω.

In what follows, we consider mainly two-dimensional solutions in the plane $q_2 = 0$ (transverse and parallel orientations) to make contact with two-dimensional numerical calculations. As an example, Figure 2 shows the neutral stability curve in the (q_1, q_3) plane for mixed parallel−transverse modes at $\epsilon = 0.04$, and for several values of the dimensionless strain amplitude γ. Recall that $q_1 = q_x(t{=}0)$ and $q_3 = q_z(t{=}0)$ define the initial orientation of the lamellae. The figure shows that the shear does not modify the neutral stability curve in the vicinity of $q_1 = 0$ (parallel orientation), whereas the curve is shifted near $q_3 = 0$ (transverse orientation). Large changes are observed for oblique wavevectors, including the complete suppression of the instability at sufficiently large values of the strain amplitude.

Above threshold, eq 4 can be solved to yield the time-dependent amplitude of the lamellar structure under oscillatory shear. We find

$$A(t) = \left\{\frac{e^{2(I(t)-c_4-c_5)}}{A(0)^2} + 6e^{2I(t)}\int_0^t dt'\, e^{-2I(t')}q^2(t')\right\}^{-1/2} \tag{13}$$

The function $I(t)$ is given by

$$I(t) = c_1 t + c_2 \sin(2\omega t) + c_3 \sin(4\omega t) + c_4 \cos(\omega t) + c_5 \cos^3(\omega t) \tag{14}$$

with

$$c_1 = \left[\frac{3q_1^4\gamma^4}{8} + \frac{(2q_0^2 + 4q_3^2 - 1)\gamma^2 q_1^2}{2} + q_0^4 + B - q_0^2\right]$$

$$c_2 = -\left[\frac{q_1^4\gamma^4 + (2q_0^2 + 4q_3^2 - 1)\gamma^2 q_1^2}{4\omega}\right], \quad c_3 = \frac{q_1^4\gamma^4}{32\omega}$$

$$c_4 = \left[\frac{(4q_0^2 - 2)\gamma q_1 q_3 + 4\gamma^3 q_1^3 q_3}{\omega}\right], \quad c_5 = -\frac{4\gamma^3 q_1^3 q_3}{3\omega}$$

We note that the stability condition eq 9 is equivalent to $c_1 = 0$. Hence, the asymptotic behavior of $A(t)$ at long times changes qualitatively depending on the sign of c_1. For $c_1 > 0$, $\lim_{t\to\infty} e^{-2I} = 0$, so that the integral in eq 13 tends to a finite constant. Since the prefactor e^{2I} diverges exponentially, $A(t)$ decays to zero. If, on the other hand, $c_1 < 0$, $A(t)$ becomes periodic at long times. To prove this statement, we first rewrite the second term inside the braces in eq 13 as

$$I(t) = 6e^{2f(t)}\int_0^t dt'\, e^{-2c_1(t'-t)-2f(t')}q^2(t') \tag{15}$$

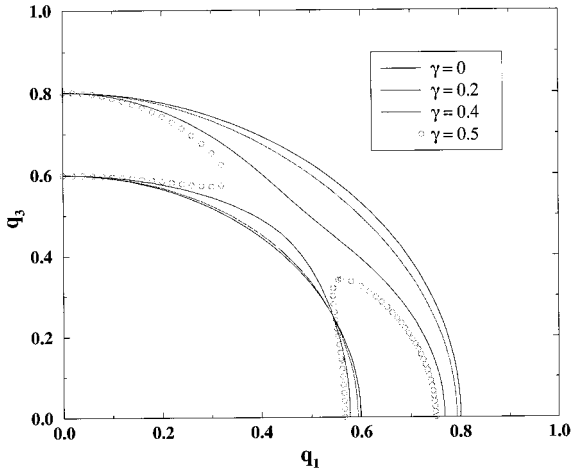

Figure 2. Neutral stability curves at $\epsilon = 0.04$ as a function of the wavenumber of the perturbation at $t = 0$ (q_1, q_3) for the values of the dimensionless strain rate γ indicated. The inner regions bounded by the various curves represent the regions in which the solution $\psi = 0$ is linearly unstable.

with $f(t') = c_2 \sin(2\omega t') + c_3 \sin(4\omega t') + c_4 \cos(\omega t') + c_5 \cos^3(\omega t')$.Since both $f(t')$ and $q^2(t')$ are periodic with period $T = 2\pi/\omega$, we can decompose eq 15 into

$$I(t) = 6e^{2f(t)}\left[\sum_{j=1}^{n} e^{2jc_1T}\int_0^T dt'\, e^{-2c_1t'-2f(t'+t)}q^2(t'+t) + e^{2c_1t}\int_0^{t-nT} dt'\, e^{-2c_1t'-2f(t')}q^2(t')\right] \tag{16}$$

where n is an integer such that $0 < t - nT < T$. In the limit of large t and with c_1 negative, the last term on the right-hand side of eq 16 vanishes while the sum $\sum_{j=1}^{n} e^{2jc_1T}$ converges to $1/(e^{-2c_1T} - 1)$. Combining eqs 13 and 16 yields an asymptotically periodic solution for $A(t)$

$$A(t) = \left[\frac{6e^{2f(t)}}{e^{-2c_1T} - 1}\int_0^T dt'\, e^{-2c_1t-'2f(t'+t)}\, q^2(t'+t)\right]^{-1/2} \tag{17}$$

The condition $c_1 = 0$ can also be understood in terms of a critical strain amplitude γ_c above which an existing lamellar structure of a given orientation at $t = 0$ will melt (i.e., $A(t)$ will decay to zero at long times). The value of γ_c that corresponds to $c_1 = 0$ is given by

$$\gamma_c = [(-b + (b^2 - 4dc)^{1/2})/2d]^{1/2} \tag{18}$$

with $b = (2q_0^2 + 4q_3^2 - 1)q_1^2/2$, $c = q_0^4 + B - q_0^2$, and $d = 3q_1^4/8$. Note again that the critical strain amplitude is independent of the angular frequency ω.

To test the approximations involved in eq 3, namely, that the wavevector **q** adiabatically follows the flow, and the single-mode truncation for small ϵ, we have undertaken a numerical solution of the model equation in a two-dimensional, square geometry (see the Appendix for the details of the numerical method). As the first example, we consider an oscillatory shear of angular frequency $\omega = 0.02$ imposed on a lamellar structure of initial wavevector $(q_1, q_3) = (0.687, 0.098)$. The critical strain amplitude for this initial orientation is $\gamma_c = 0.695$. Figure 3 shows the temporal evolution of $A(t)$ for two values of γ, one larger and one smaller than γ_c. The solid lines are the predictions of eq 13, and the symbols are

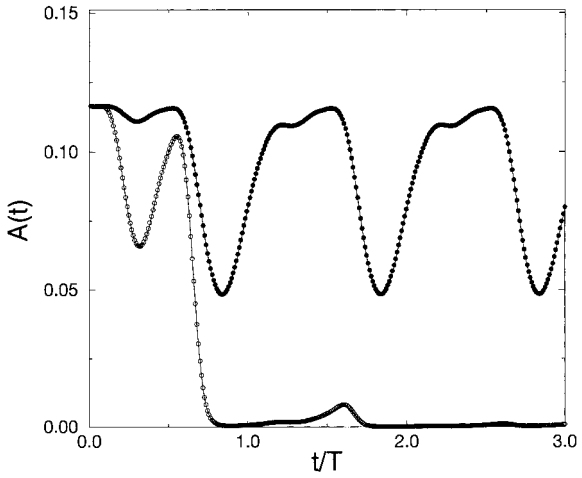

Figure 3. Temporal evolution of the amplitude $A(t)$ of the single-mode solution given in eq 13 for an oscillatory shear (solid lines), along with the corresponding numerical solution of the full model for $\epsilon = 0.04$, $\omega = 0.02$, and $\gamma = 0.5$ (●) and $\gamma = 0.75$ (○). Time has been scaled by the period of the shear $T = 2\pi/\omega$. For $\gamma = 0.75$, the initial periodic pattern is unstable against uniform melting and the amplitude $A(t)$ decreases to zero. On the other hand, for $\gamma = 0.5$ a spatially periodic solution is stable, and after a transient, $A(t)$ becomes a periodic function of time (eq 17).

the results of the numerical calculation. The agreement in both cases is excellent.

4. Secondary Instabilities of the Lamellar Pattern

To address the stability of the lamellar pattern, we next consider long-wavelength perturbations of the base state with wavevector $\mathbf{Q} = (Q_1, Q_2, Q_3)$ such that its components are also constant in the sheared frame of reference. Close to threshold, perturbations evolve in a slow time scale compared to the inverse frequency of the shear. We therefore assume that the wavenumber of any long wave perturbation would adiabatically follow the imposed flow. Specifically, we consider a solution of the form

$$\psi(\mathbf{r}, t) = [A(t) + \delta A_+ e^{i\mathbf{Q}\cdot\mathbf{r}} + \delta A_- e^{-i\mathbf{Q}\cdot\mathbf{r}}]e^{i\mathbf{q}\cdot\mathbf{r}} + \text{cc} \quad (19)$$

where $A(t)$ is the nonlinear solution obtained in section 3. Substituting eq 19 into eq 2, and linearizing with respect to the amplitudes δA_+ and δA_-, we find

$$\frac{\partial}{\partial t}\begin{bmatrix}\delta A_+ \\ \delta A_-\end{bmatrix} = L(t)\begin{bmatrix}\delta A_+ \\ \delta A_-^*\end{bmatrix} \quad (20)$$

with

$$L(t) = \begin{bmatrix}-l_+ - l_+^2 - B + 6A(t)^2 l_+ & 3A(t)^2 l_+ \\ 3A(t)^2 l_- & -l_- - l_-^2 - B + 6A(t)^2 l_-\end{bmatrix}$$

and $l_\pm = -(\mathbf{q} \pm \mathbf{Q})^2 = -(1 + a(t)^2)(q_1 \pm Q_1)^2 + 2a(t)(q_1 \pm Q_1)(q_3 \pm Q_3) - (q_2 \pm Q_2)^2 - (q_3 \pm Q_3)^2$. In general, the matrix elements L_{ij} are complicated functions of time, and we have not attempted to solve eq 20 analytically. For $\gamma < \gamma_c$ the operator L contains terms that are periodic in time and decaying transients. At long enough times, $A(t)$ is given by eq 17, and the linear system eq 20 has periodic coefficients. Hence, it reduces to a two-dimensional Floquet problem for the amplitudes δA_+ and δA_-^*.[26]

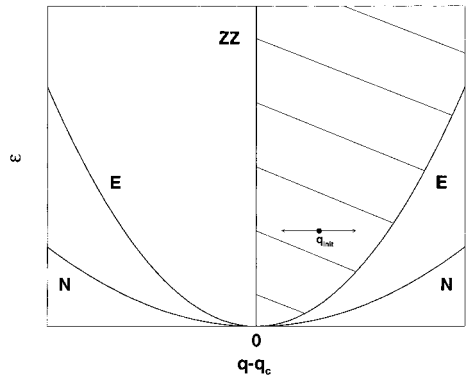

Figure 4. Schematic representation of the neutral stability curve (N) and the Eckhaus (E) and zigzag (ZZ) boundaries for the case of no flow. Within the shaded region the lamellar pattern is linearly stable. The effect of an imposed shear on a uniform lamellar structure can be qualitatively understood as the displacement of the state point along a line of constant ϵ. This representation, however, fails to give the correct location of the stability boundaries given in the text.

To gain some insight into the stability problem, we first briefly review the known results for zero shear.[11,12] In this case $A(t)$ is a constant, and the matrix elements of $L(t)$ are independent of time. An eigenvalue problem results by considering solutions of eq 20 of the form $\delta A_\pm \approx e^{\sigma_+ t} + e^{\sigma_- t}$, and instability follows when either eigenvalue is positive. Two modes of instability are obtained: a zigzag (ZZ) mode that leads to a transverse modulation of the lamellae ($\mathbf{Q}\cdot\mathbf{q} = 0$), and an Eckhaus (E) mode that is purely longitudinal in nature ($\mathbf{Q}\cdot\mathbf{q} = Qq$). In the zigzag case, $\sigma_+(\mathbf{Q})$ has a maximum at

$$Q^2_{\text{max,ZZ}} = \frac{1 - 2q^2 - 3A^2}{2} \quad (21)$$

The eigenvalue $\sigma_+(\mathbf{Q})$ changes sign on the line $q = q_c$, which therefore defines the zigzag stability boundary. In the Eckhaus case, we find after some straightforward algebra that the perturbation with the largest growth rate is

$$Q^2_{\text{max,E}} = \frac{64\delta q^4 - (\epsilon - 4\delta q^2)^2}{64\delta q^2} \quad (22)$$

with $\delta q = q - q_c$. Therefore, the Eckhaus stability boundary is given by $\epsilon = 12\delta q^2$. These results are schematically summarized in Figure 4. The hatched area is the region of stability of a lamellar solution in the absence of shear flow. It is worth pointing out that this stability diagram is identical to that of the Swift−Hohenberg model of Rayleigh−Bénard convection.[15] Shiwa[12] has recently shown that, in the weak-segregation limit ($\epsilon \ll 1$), and in the absence of shear flow, the amplitude equation describing slow modulations of a lamellar solution is the same as the amplitude equation of the Swift−Hohenberg model near onset of convection. The same stability diagram has been derived by Kodama and Doi[11] by examining free energy changes upon distortion of a lamellar pattern.

We now return to the Floquet problem of eq 20 when $A(t)$ is a periodic function of time (eq 17). Since $A(t+T) = A(t)$ ($T = 2\pi/\omega$), the solution of eq 20 is given by

$$\begin{bmatrix}\delta A_+\\ \delta A_-\end{bmatrix} = e^{\sigma t}\begin{bmatrix}\phi_+(t)\\ \phi_-(t)\end{bmatrix} \tag{23}$$

with $\phi_\pm(t+T) = \phi_\pm(t)$. Equation 20 is then transformed to an eigenvalue problem within $(0, T)$

$$\frac{\partial}{\partial t}\begin{bmatrix}\phi_+(t)\\ \phi_-(t)\end{bmatrix} = -\sigma\begin{bmatrix}\phi_+(t)\\ \phi_-(t)\end{bmatrix} + L(t)\begin{bmatrix}\phi_+(t)\\ \phi_-(t)\end{bmatrix} \tag{24}$$

Given that the function $A(t)$ is quite complicated, we have solved this eigenvalue problem numerically. The eigenvalue σ can depend in principle on the wavevector of the base state $\mathbf{q}$, on the wavevector of the perturbation $\mathbf{Q}$, and on the amplitude γ and frequency ω of the shear. For ease of presentation, we have focused on the case $\epsilon = 0.04$, although extension to other values of ϵ is straightforward.

Figures 5 and 6 summarize our results for the cases $\gamma = 0.2$ and $\gamma = 0.4$, respectively, and show the stability boundaries in the plane (q_1, q_3), as well as the neutral stability curve already shown in Figure 2. As before, (q_1, q_3) is the wavevector of the lamellar structure at $t = 0$. At fixed ϵ, γ, and ω, these curves have been obtained by determining the loci of $\mathbf{q}$ at which the function $\sigma(\mathbf{Q})$ changes from a maximum to a saddle point at $\mathbf{Q} = 0$. First, we note that any orientation of the lamellar pattern that is not initially close to either parallel or transverse is unstable to moderate shears. Second, there is a weak dependence of the stability boundaries on frequency. The dependence is more pronounced for frequencies on the order of the linear growth rate. The change in the location of the stability boundaries in this range can be traced back to changes of $A(t)$ with frequency. At lower frequencies, $A(t)$ adiabatically follows $q(t)$, and the dependence on ω approximately scales out. At higher frequencies, $A(t)$ almost becomes independent of time, and the stability boundaries again become only weakly dependent on ω. Finally, and contrary to the case of no shear, the reciprocal basis vectors are not time-independent. Since the components of both $\mathbf{q}$ and $\mathbf{Q}$ are independent of time in the sheared frame, their mutual angle is not (except for the case in which they are parallel). However, the secondary instability is of the longitudinal type when either $q_1 = 0$ or $q_3 = 0$. Otherwise, the angle between $\mathbf{q}$ and $\mathbf{Q}$ is time-dependent.

The cases discussed up to now concern long-wavelength instabilities of the base periodic pattern that are associated with the broken translational symmetry of the original system by the appearance of a periodic pattern. We now show that it is possible to obtain analytical expressions for the stability boundaries against finite-wavelength perturbations that may have some experimental relevance as well. In some experimental protocols, the lamellar pattern is first obtained in the absence of shear. The resulting configuration comprises regions or domains of locally parallel lamellae but with a continuous distribution of orientations. A shear flow is then initiated and the reorientation of the pattern studied as a function of time. The pattern obtained in the absence of shear may now be unstable to several finite-wavenumber perturbations that would not have been observable in the case in which flow is present throughout the ordering process. In the latter case the unstable orientations would have decayed away during the process of formation of the lamellae. In addition, the approximation that we derive below is generally

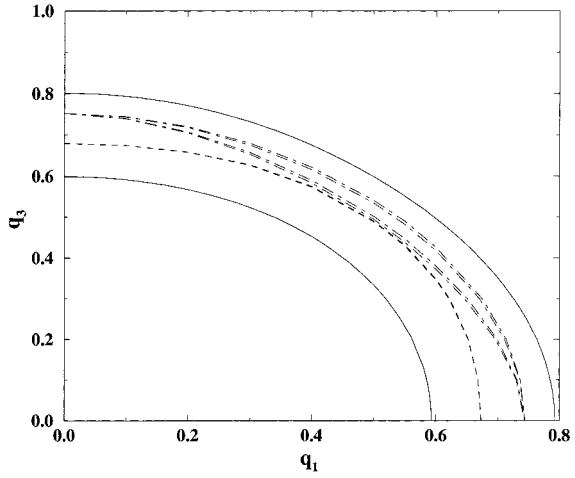

Figure 5. Stability diagram of a lamellar pattern under oscillatory shear of amplitude $\gamma = 0.2$ and frequencies $\omega = 0.0025$, 0.01, 0.05, and 0.25, at $\epsilon = 0.04$. The solid lines show the neutral stability curve. The bottom (dashed) line is the common stability boundary for the four frequencies shown. The top (dotted−dashed) lines are ordered from top to bottom in decreasing order of frequency (the region of stability is larger at higher frequencies). Note also that the largest change occurs between $\omega = 0.01$ and $\omega = 0.05$ as discussed in the text.

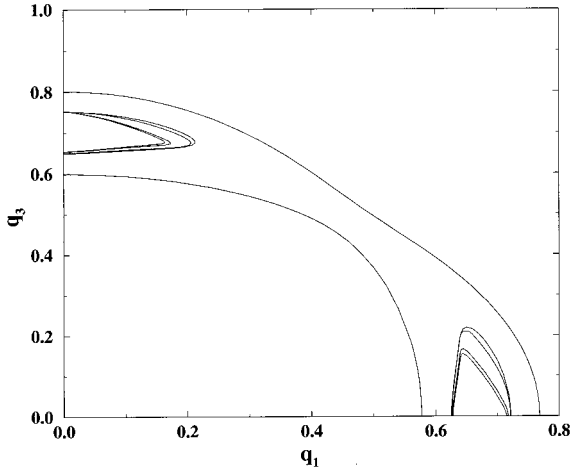

Figure 6. Stability diagram of the lamellar pattern under oscillatory shear of amplitude $\gamma = 0.4$ and frequencies $\omega = 0.0025$, 0.01, 0.05, and 0.25, at $\epsilon = 0.04$. The outer solid lines show the neutral stability curve. The inner solid lines bound the regions of stability of the lamellar structure against long-wavelength perturbations for the four frequencies given, with the region of stability increasing with frequency. Note that the largest change occurs between $\omega = 0.01$ and $\omega = 0.05$ as discussed in the text.

valid when Q_3 cannot approach zero, as is the case in a system of finite extent in the direction of the velocity gradient.

We first define the following linear transformation

$$\begin{bmatrix}\delta_+\\ \delta_-\end{bmatrix} = \begin{bmatrix}\dfrac{3A(t)^2 l_-}{\sigma_+ - \sigma_-} & \dfrac{\sigma_+ - \sigma_- + L_{22} - L_{11}}{2(\sigma_+ - \sigma_-)}\\ -\dfrac{3A(t)2l_-}{\sigma_+ - \sigma_-} & \dfrac{\sigma_+ - \sigma_- + L_{11} - L_{22}}{2(\sigma_+ - \sigma_-)}\end{bmatrix}\begin{bmatrix}\delta A_+\\ \delta A_-\end{bmatrix} = T(t)\begin{bmatrix}\delta A_+\\ \delta A_-\end{bmatrix} \tag{25}$$

which diagonalizes matrix $L(t)$, and where

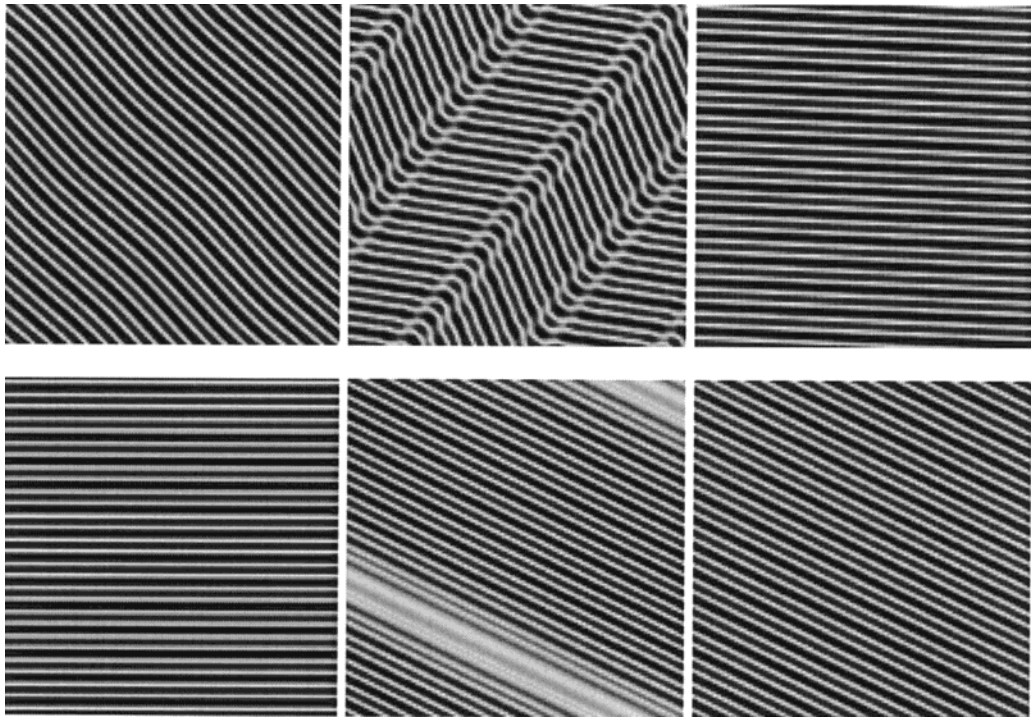

Figure 7. Results of the numerical integration of the model equation to show the instability of a lamellar pattern (shown in gray scale). The field γ shown in this figure has been transformed back to the laboratory frame of reference. Top, left to right: instability approximately of the zigzag type, followed by kink band formation and reconnection, leading to a different orientation. Bottom: instability approximately of the Eckhaus type, leading to the disappearance of a pair of lamellae.

$$\sigma_{\pm}(t) = \frac{L_{11} + L_{22} \pm [(L_{11} - L_{22})^2 + 36 l_+ l_- A(t)^4]^{1/2}}{2} \tag{26}$$

Combining eqs 20 and 25, we find

$$\frac{\partial}{\partial t}\begin{bmatrix}\delta_+(t)\\ \delta_-(t)\end{bmatrix} = \begin{bmatrix}\sigma_+ & 0\\ 0 & \sigma_-\end{bmatrix}\begin{bmatrix}\delta_+\\ \delta_-\end{bmatrix} - \frac{A(t)^2 l_-}{\sigma_+ - \sigma_-}\begin{bmatrix}\dot{M}_1 & -\dot{M}_2\\ -\dot{M}_1 & \dot{M}_2\end{bmatrix}\begin{bmatrix}\delta_+\\ \delta_-\end{bmatrix} \tag{27}$$

where $\dot{M}_1 = (\partial/\partial t)[(\sigma_+ - \sigma_- + L_{11} - L_{22})/2A^2 l_-]$ and $\dot{M}_2 = (\partial/\partial t)[(\sigma_- - \sigma_+ + L_{11} - L_{22})/2A^2 l_-]$. For finite Q, $36A(t)^4 l_+ l_-/(L_{11} - L_{22})^2 \ll 1$. Assuming $L_{11} - L_{22} > 0$ (the other case leads to no extra complications), $\sigma_+ = L_{11}$ and $\sigma_- = L_{22}$. Also $M_1 = (L_{11} - L_{22})/A^2 l_-$ and $M_2 = 0$ so that the equation for δ_+ decouples from the equation for δ_-. The solution for δ_+ is

$$\delta_+(t) = \delta_+(0) \mathrm{e}^{\int_0^t (\sigma_+ - (\partial/\partial t') \ln[(L_{22} - L_{11})/A^2 l_-]) \mathrm{d}t'} \tag{28}$$

The stability boundary is defined by $\bar{\sigma} = \int_0^T (\sigma_+ - (\partial/\partial t') \ln[L_{22} - L_{11}/A^2 l_-])\, \mathrm{d}t' = \int_0^T \sigma_+ \, \mathrm{d}t' = 0$. We have checked that this stability condition agrees with the numerical stability analysis based on eq 24 for finite Q.

We finish by illustrating the reorientation dynamics of the lamellar structure following a long-wavelength instability by direct numerical solution of the governing equation. We focus on the region in which the uniform lamellar structure is linearly unstable. The first example discussed concerns a lamellar structure of initial wavenumber $(q_1, q_3) = (-0.4908, 0.4908)$ being sheared periodically with an amplitude $\gamma = 1$. Figure 7 (top row) shows the sequence of configurations obtained when $\omega = 5 \times 10^{-6}$. A long-wavelength transverse modulation of the lamellae is observed (Figure 7, top left). Subsequent growth leads to the formation of a forward kink band similar to that recently observed experimentally (Figure 7, top center).[27,28] As the strain grows larger, the kink band disappears, leaving behind a lamellar structure without any defects and oriented differently relative to the shear (Figure 7, top right).

In the second example (Figure 7, bottom row), a structure initially transverse to the flow is being sheared periodically with an amplitude $\gamma = 1$ and a frequency $\omega = 5 \times 10^{-7}$. A longitudinal perturbation is clearly visible that manifests itself by local compression and dilation of the structure, leading to the disappearance of a pair of lamellae. The overall result is an increase in the lamellar spacing.

In summary, we have obtained a nonlinear solution of the model equations that govern the formation of a lamellar structure in the weak-segregation limit. The solution is a periodic lamellar structure with a time-dependent wavevector that adiabatically follows the imposed shear flow, and a time-dependent amplitude which we have computed for the cases of steady and oscillatory shears. In the case of an oscillatory shear, the periodic solution only exists for a range of orientations of the lamellae relative to the shear direction. The width of the region depends on the shear amplitude but not on its frequency. Long-wavelength secondary instabilities further reduce the range of existence of stable lamellar solutions. The corresponding stability boundaries depend on the shear amplitude and its frequency. We next plan to examine the stability of the nonlinear solution presented in this paper when neither osmotic stresses nor viscosity contrast is neglected.

Acknowledgment. This research has been supported by the U.S. Department of Energy, Contract No. DE-FG05-95ER14566, and also in part by the Super-

computer Computations Research Institute, which is partially funded by the U.S. Department of Energy, Contract No. DE-FC05-85ER25000. F.D. is supported by the Microgravity Science and Applications Division of NASA under Contract No. NAG3-1885.

Appendix. Numerical Algorithm

We use a pseudospectral technique to solve eq 2 in two spatial dimensions and in the sheared frame with periodic boundary conditions along both directions. Equation 2 can be written as

$$\partial\tilde{\psi}/\partial t = \sigma(t)\tilde{\psi} - q^2(t)\tilde{\psi}^3 \tag{29}$$

where $\sigma(t) = q^2(t) - q^4(t) - B$ and $q^2(t) = q_1{}^2 + [a(t)q_1 - q_3]^2$. The algorithm we use, due to Cross et al.,[29] is obtained by first multiplying both sides of eq 29 by $\exp(-\sigma(t')t')$ and integrating over t'. This gives

$$\exp(-\sigma(t)t')\tilde{\psi}|_t^{t+\Delta t} = -q^2(t)\int_t^{t+\Delta t} \mathrm{d}t'\ \tilde{\psi}^3(t')\exp(-\sigma(t)t') \tag{30}$$

where we have assumed $\sigma(t') \approx \sigma(t)$ and $q^2(t') \approx q^2(t)$. Next, we write the nonlinear term $\tilde{\psi}^3(t')$ as a linear function of t' in the interval $t \le t' \le t + \Delta t$, i.e.

$$\tilde{\psi}^3(t') \approx \tilde{\psi}^3(t) + \frac{\tilde{\psi}^3(t+\Delta t) - \tilde{\psi}^3(t)}{\Delta t}(t - t') \tag{31}$$

Combining the last two equations finally yields

$$\tilde{\psi}(t+\Delta t) = \exp(\sigma(t)\,\Delta t)\,\tilde{\psi}(t) - q^2(t)\tilde{\psi}^3(t) \times \left[\frac{\exp(\sigma(t)\,\Delta t) - 1}{\sigma(t)}\right] - q^2(t)\left[\frac{\tilde{\psi}^3(t+\Delta t) - \tilde{\psi}^3(t)}{\Delta t}\right] \times \left[\frac{\exp(\sigma(t)\,\Delta t) - (1 + \sigma(t)\,\Delta t)}{\sigma^2(t)}\right] \tag{32}$$

Equation 32 is first evaluated with the last term on its right-hand side set to zero. The resulting value for $\tilde{\psi}(t+\Delta t)$ is then used to estimate $\tilde{\psi}^3(t+\Delta t)$. Equation 32 is finally applied a second time with all three terms on its right-hand side now included in the calculation. The fact that the nonlinear terms are integrated using an explicit procedure in time limits the size of the time step Δt that can be used in simulations of the model.

All the numerical results presented in this paper were obtained in the sheared frame of reference with 128 × 128 spectral modes. We have chosen $B = 0.23$ (which corresponds to $\epsilon = 0.04$) and a time step of maximum size $\Delta t = 0.2$, for which no numerical instability was observed. The initial condition $\psi(\mathbf{r},t=0)$ is, unless otherwise noted, a lamellar structure obtained by numerical integration of eq 32 with $a(t) = 0$ (no shear) starting from a random initial condition (a Gaussian distribution for ψ of zero mean and small variance), for approximately 300 000 iterations until a stationary lamellar structure is reached.

References and Notes

(1) Chen, Z.-R.; Issaian, A.; Kornfield, J.; Smith, S.; Grothaus, J.; Satkowski, M. *Macromolecules* **1997**, *30*, 7096.
(2) Leibler, L. *Macromolecules* **1980**, *13*, 1602.
(3) Ohta, T.; Kawasaki, K. *Macromolecules* **1986**, *19*, 2621.
(4) Seul, M.; Andelman, D. *Science* **1957**, *267*, 476.
(5) Bates, F.; Fredrickson, G. *Annu. Rev. Phys. Chem*. **1990**, *41*, 525.
(6) Matsen, M.; Schick, M. *Phys. Rev. Lett*. **1994**, *72*, 1994.
(7) Laradji, M.; Shi, A.-C.; Noolandi, J.; Desai, R. *Macromolecules* **1997**, *30*, 3242.
(8) Netz, R.; Andelman, D.; Schick, M. *Phys. Rev. Lett*. **1997**, *79*, 1058.
(9) Villain-Guillot, S.; Netz, R.; Andelman, D.; Schick, M. *Physica A* **1998**, *249*, 285.
(10) Fredrickson, G. *J. Rheol*. **1994**, *38*, 1045.
(11) Kodama, H.; Doi, M. *Macromolecules* **1996**, *29*, 2652.
(12) Shiwa, Y. *Phys. Lett. A* **1997**, *228*, 279.
(13) Swift, J.; Hohenberg, P. *Phys. Rev. A* **1977**, *15*, 319.
(14) Greenside, H.; Cross, M. *Phys. Rev. A* **1985**, *31*, 2492.
(15) Cross, M.; Hohenberg, P. *Rev. Mod. Phys*. **1993**, *65*, 851.
(16) Elder, K.; Viñals, J.; Grant, M. *Phys. Rev. Lett*. **1992**, *68*, 3024.
(17) Cross, M.; Meiron, D. *Phys. Rev. Lett*. **1995**, *75*, 2152.
(18) Koppi, K. A.; Tirrell, M.; Bates, F. B.; Almdal, K.; Colby, R. H. *J. Phys. II* **1992**, *2*, 1941.
(19) Gunton, J. D.; San Miguel, M.; Sahni, P. S. In *Kinetics of first order phase transitions*; Domb, C., Lebowitz, J., Eds.; Academic: London, 1983; Vol. 8.
(20) Fredrickson, G.; Helfand, E. *J. Chem. Phys*. **1988**, *89*, 5890.
(21) Helfand, E.; Fredrickson, G. H. *Phys. Rev. Lett*. **1989**, *62*, 2468.
(22) Gurtin, M. E.; Polignone, D.; Viñals, J. *Math. Mod. Methods Appl. Sci*. **1996**, *6*, 815.
(23) Anderson, D.; McFadden, G.; Wheeler, A. *Annu. Rev. Fluid Mech*. **1998**, *30*, 139.
(24) Qi, S.; Wang, Z.-G. *Phys. Rev. Lett*. **1996**, *76*, 1679; *Phys. Rev. E* **1997**, *55*, 1682; *Polymer* **1998**, *39*, 4639.
(25) Cates, M.; Milner, S. *Phys. Rev. Lett*. **1989**, *62*, 1856.
(26) Iooss, G.; Joseph, D. *Elementary Stability and Bifurcation Theory*; Springer-Verlag: New York, 1990.
(27) Polis, D.; Winey, K. *Macromolecules* **1996**, *29*, 8180.
(28) Polis, D.; Winey, K. *Macromolecules* **1998**, *31*, 3617.
(29) Cross, M.; Meiron, D.; Tu, Y. *Chaos* **1994**, *4*, 607.

MA990448O